

Combined forced and natural convection heat transfer for upward flow in a uniformly heated, vertical pipe

HIROAKI TANAKA, SHIGEO MARUYAMA and SHUNICHI HATANO
Department of Mechanical Engineering, University of Tokyo, Bunkyo-ku, Tokyo 113, Japan

(Received 24 February 1986 and in final form 21 April 1986)

Abstract—For predicting the fully developed upward flow in a uniformly heated, vertical pipe by taking account of the buoyancy force, the k - ϵ models of turbulence for low Reynolds number flows were adopted. The regime map for forced, mixed and natural convections as well as for laminar and turbulent flows was plotted from the numerical predictions. At the same time, experiments were carried out at Reynolds numbers of 3000 and 5000, with the Grashof number varying over a wide range, by using pressurized nitrogen gas as a test fluid. In agreement with the prediction, buoyancy-induced impairment of heat transfer was correctly measured in the mixed convection regime. Furthermore, from hot-wire measurements, complete laminarization was demonstrated in the mixed-convection region at a Reynolds number of 3000.

INTRODUCTION

IN CERTAIN practical equipment, forced and natural convection may appear combined together. In these cases, it is of prime interest to discriminate which convection regime is dominant as well as to resolve how much the heat transfer coefficient contributes. For example, in the case of a hypothetical loss-of-coolant accident of a pressurized water reactor (PWR), cold water will be supplied to the downcomer, and the mean flow rate there will often decrease. In that case, accurate prediction of the heat transfer coefficient is needed to estimate the magnitude of the thermal shock that the reactor wall will suffer. Other examples are given by solar heat collectors, high-temperature gas-cooled nuclear reactors, supercritical boilers, and cooling of electronic equipment.

Combined forced and natural convection, especially in turbulent flow, is not fully explored. Until recently, the methods most often used to discriminate between forced, mixed and natural convections have been to refer to the classical regime map suggested by Metais and Eckert [1], or to rely on the more classical rule proposed by McAdams: one calculates the heat transfer coefficient from both forced-convection and natural-convection relations and then uses the larger value [2]. Shitsman [3] compared heat transfer data for upward and downward flows of water in a heated tube at supercritical pressures and reported that, in the case of upward flow, the temperature distribution along the tube sometimes showed a local temperature rise due to the local impairment of heat transfer, while, for downward flow, heat transfer was stable and better than the upward flow under the same flow rate and the same heat flux. With a view to explaining these phenomena by the effect of buoyancy force, a number of researches in relation to the combined convection

have been pushed forward in the field of heat transfer for supercritical fluids, until Watts and Chou [4] recently presented heat transfer correlations performing experiments over a wide range of parameters with supercritical pressure water. A detailed review of the work to date is available in Jackson and Hall [5]. The fruits of these researches are the discrimination equations between forced, mixed and natural convection in a vertical pipe presented by Hall and Jackson [5, 6] and Tanaka *et al.* [7, 8], as well as the respective equations for the heat transfer correlation in each regime [4, 9]. However, some of these results cannot be easily accepted as universal, since most of them were based on experiments performed with supercritical pressure fluids which involved a large change of physical properties. Other experiments with air or water [9, 10], on the other hand, needed very large experimental facilities to attain large Grashof numbers, and they could only cover fairly limited ranges of the experimental Reynolds and Grashof numbers.

Abdelmeguid and Spalding [11] applied, for the first time, a two-equation model of turbulence to flow and heat transfer in pipes with buoyancy effects. They were fairly successful in reproducing the difference of heat transfer between upward and downward flows revealed by experiments, as well as predicting velocity and temperature distributions in agreement with the experimental results obtained for the upward flow of mercury in a heated pipe [12]. However, their model adopted a simple treatment near the wall, utilizing the wall function; an approach which seems open to question.

Flow systems in a vertical pipe are divided into two kinds. Those in which the buoyancy force acts in the same direction as the flow (e.g. a heated upward flow or a cooled downward flow) are termed 'aiding' flows.

Averaging this definition equation over the cross-section results in the pressure term together with the buoyancy term in equation (1). In the case of the uniformly heated flow, it may be controversial to assume the fully developed state, since the bulk-fluid temperature increases constantly along the flow. However, as a way of realizing a flow with a prescribed Grashof number, we can imagine a world where the gravitational acceleration is so large that the wall heat-flux can be taken to be small enough for the bulk-fluid temperature rise to become negligible. Under such a condition, the fully developed state would certainly be attained. Integrating equations (1) and (2) over the cross-section of the pipe yields

$$-\frac{dp_a}{dx} = \frac{4\tau_w}{D}, \quad \frac{dT_m}{dx} = \frac{4q_w}{c_p \rho D U_m}. \quad (3)$$

As turbulence models, we adopt the $k-\varepsilon$ model of Jones and Launder [14, 15] and its modified version by Kawamura [16]. The latter was devised searching for better predictability in transient turbulent pipe flows. Both of the models are expressed as

$$0 = \frac{1}{r} \frac{d}{dr} \left[\left(\frac{\mu_t}{\sigma_k} + \mu \right) r \frac{dk}{dr} \right] + \mu_t \left(\frac{dU}{dr} \right)^2 - \rho \varepsilon - 2\mu \left(\frac{d\sqrt{k}}{dr} \right)^2 \quad (4)$$

$$0 = \frac{1}{r} \frac{d}{dr} \left[\left(\frac{\mu_t}{\sigma_\varepsilon} + \mu \right) r \frac{d\varepsilon}{dr} \right] + C_1 \frac{\varepsilon}{k} \mu_t \left(\frac{dU}{dr} \right)^2 - C_2 \rho \frac{\varepsilon^2}{k} + C_3 \nu \mu_t \left(\frac{d^2 U}{dr^2} \right)^2 \quad (5)$$

where, in the case of the model by Jones and Launder,

$$\begin{aligned} \mu_t &= C_\mu f_\mu \rho k^2 / \varepsilon & C_2 &= 2.0 [1 - 0.3 \exp(-R_t^2)] \\ \lambda_t &= \mu_t c_p / \sigma_t & C_3 &= 2.0 \\ \sigma_k &= 1.0 & C_\mu &= 0.09 \\ \sigma_\varepsilon &= 1.3 & f_\mu &= \exp[-2.5/(1 + R_t/50)] \\ C_1 &= 1.55 & R_t &= k^2 / (\nu \varepsilon). \end{aligned}$$

Kawamura has modified only the coefficient C_1 as follows

$$C_1 = 1.5 \{1 + 0.15 \exp[-(R_t/50)^2]\}.$$

The turbulent Prandtl number σ_t is assumed to be constant at 0.9. The buoyancy-effect terms due to turbulent mixing have been ignored in both k and ε equations, because the main turbulent heat flux in this system is normal to the gravitational acceleration and the temperature gradient in the direction of gravity $\partial T / \partial x$ is assumed to be small.

The boundary conditions for equations (1), (2), (4)

and (5) are

$$r = D/2:$$

$$U = 0, \quad \frac{dU}{dr} = -\tau_w / \mu, \quad T = T_w, \quad \frac{dT}{dr} = \frac{q_w}{\lambda}$$

$$r = 0: \quad \frac{dk}{dr} = \frac{d\varepsilon}{dr} = 0$$

$$r = D/2: \quad k = \varepsilon = 0.$$

For the convenience of computation procedure, the following additional boundary conditions as to the symmetry of profiles, which are already included in the implication of equation (3), are introduced.

$$r = 0: \quad \frac{dU}{dr} = \frac{dT}{dr} = 0.$$

Equations (1), (2), (4) and (5) are discretized on 100 grid nodes distributed with larger concentration near the wall, by means of the control-volume method described by Patankar [17]. The initial profiles for iterative solution are set as follows assuming the fully developed isothermal flow at the given Reynolds number, i.e. the velocity profile assumes the 1/7th power law with linear part near the wall, the turbulence kinetic energy k is given a constant value of $3u^*{}^2$ with a modification of $k = u^*{}^4 y^2 / \nu^2$ near the wall, the dissipation rate is assumed to be $0.41k^{3/2}/y$, and finally the temperature is set constant as $T = T_m$.

Numerical results

Eight Reynolds numbers were selected in a range between 1000 and 25,000. For each Reynolds number, the Grashof number was varied so as to cover all the three regimes of forced, mixed and natural convection. Here, the Reynolds number and the Grashof number are defined as

$$Re = \frac{U_m D}{\nu_f}, \quad Gr = \frac{g \beta (T_f - T_m) D^3}{\nu_f^2} \quad (6)$$

where the subscript f refers to the value at the film temperature $T_f = (T_w + T_m)/2$. These definitions are consistent with those used in the data reductions described later, and assume application of the results to the case with a large change of physical properties [7]. From the calculated results, shown in Fig. 1, variations of the Nusselt number with the Grashof number, for three Reynolds numbers of 3000, 5000 and 10,000, are obtained. Here, the Nusselt number is defined as

$$Nu = \frac{hD}{\lambda_f} = \frac{q_w}{T_w - T_m} \cdot \frac{D}{\lambda_f}. \quad (7)$$

At the lowest Grashof number for each calculation, almost pure forced convection seems to be realized. As the Grashof number increases, the Nusselt number begins to decrease, takes a minimum, and then increases almost in proportion to the 0.45th power of

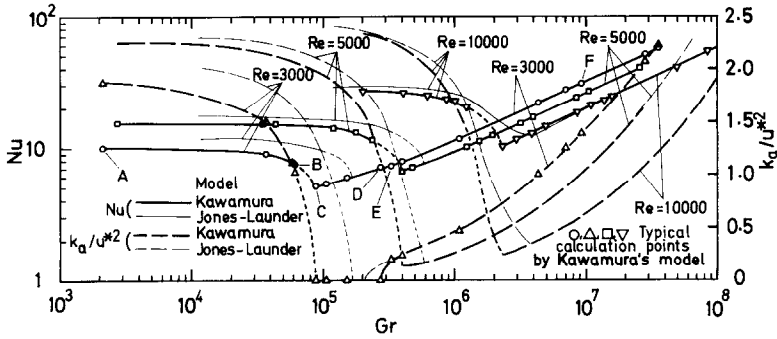


FIG. 1. Calculated variations of Nusselt number and cross-sectionally averaged turbulence kinetic energy with Grashof number, for three Reynolds numbers.

the Grashof number. From the calculated results for $Re = 3000$ with Kawamura's model, the velocity profiles together with the shear-stress distributions at six typical Grashof numbers are shown in Fig. 2. This figure clearly shows change of the flow state from forced, via mixed, to natural convection. In Fig. 1, the

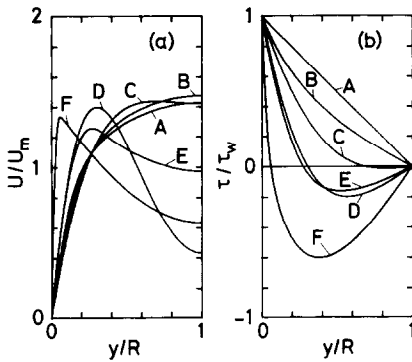


FIG. 2. (a) Velocity and (b) shear-stress distributions at various Grashof numbers under a constant Reynolds number of 3000, predicted by Kawamura's model: A, $Gr = 2.1 \times 10^3$, turbulent; B, $Gr = 6.1 \times 10^4$, turbulent; C, $Gr = 8.8 \times 10^4$, laminar; D, $Gr = 2.7 \times 10^5$, laminar; E, $Gr = 3.3 \times 10^5$, turbulent; F, $Gr = 9.2 \times 10^6$, turbulent.

cross-sectionally averaged turbulence kinetic energy k_a , nondimensionalized by the square of the friction velocity $u^* = \sqrt{\tau_w/\rho}$, is also plotted. The curve corresponding to the case of $Re = 3000$ and with Kawamura's model reveals that the flow becomes completely laminar in the range of Grashof numbers $8.8 \times 10^4 - 2.7 \times 10^5$ (corresponding to points C and D in Fig. 1 and distributions C and D in Fig. 2). Further, it turns out that in the cases of the larger Reynolds numbers of 5000 and 10,000, the turbulence energy decreases considerably, though it does not vanish, just in the range where the Nusselt number decreases. A jump of the calculation point, indicated by a dotted line in Fig. 1, appears in the range where the Nusselt number decreases rapidly. This is caused by the nature of the systematic calculation which was done with increasing wall heat flux q_w step by step under a given flow rate. Then, the balance of heat flux at the wall becomes unstable in the region where the heat transfer characteristics change more steeply than $Nu \propto Gr^{-1}$; because Gr is proportional to the moving parameter $(T_w - T_m)$, while Nu is reciprocally proportional to it.

Figure 3 is the numerically predicted regime map for combined forced and natural convection, plotted in the Reynolds number against Grashof number plane. The upper left part of Fig. 3 naturally supports

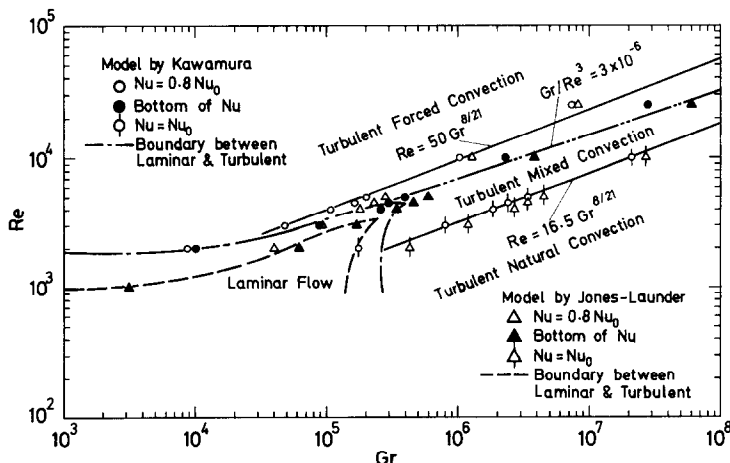


FIG. 3. Predicted regime map for combined forced and natural convection.

the forced-convection regime, while the lower right encourages natural convection. The boundaries between forced, mixed and natural convection are determined from those Nusselt number variations as are plotted in Fig. 1 by the following rule. Here, the Nusselt number in the complete forced-convection condition is denoted by Nu_0 . Each of the open circular and triangular symbols in Fig. 3 (referring to Kawamura's model and Jones and Launder's model, respectively) indicates the point at which the Nusselt number becomes $0.8Nu_0$ with increasing the Grashof number from zero. This point is assumed to define the boundary between forced and mixed convections. As the Grashof number is further increased, the Nusselt number meets the minimum value at the point denoted by a solid symbol, and then it recovers to Nu_0 at the point indicated by a symbol with a vertical tick. The last point is regarded as the boundary between mixed and natural convection. Two straight full-lines drawn in Fig. 3 represent the following discrimination equations between turbulent, forced and mixed convection and also between turbulent, mixed and natural convection, which were derived from considerations of the shear-stress distributions near the wall by Tanaka *et al.* [7, 8]

$$Re = 50 Gr^{8/21} \quad (8)$$

$$Re = 16.5 Gr^{8/21}. \quad (9)$$

The boundaries predicted numerically by both of the turbulence models prove to agree well with equations (8) and (9).

If the turbulence kinetic energy k converges to zero over the whole cross-section during iterative solution, the flow is considered to be in the laminar regime. In this way the boundary between laminar and turbulent flows can be determined as shown in Fig. 3. Here, the Jones–Launder model gives the transition Reynolds number of isothermal flow within a range between 900 and 1000, while that from Kawamura's model falls between 1800 and 1900. These values are slightly lower than those reported by the originators, presumably because of the difference in the calculation procedures. Originating from the difference in the transition Reynolds number of isothermal flow, there is a slight shift between the two laminar–turbulent boundaries predicted from the two turbulence models. Here, it must be noted that the laminar regime makes inroads right into the turbulent mixed-convection region. This is because, in the mixed-convection regime, the local shear stress near the wall decreases sharply from the value at the wall owing to the buoyancy effect [see Fig. 2(b)], which results in the decrease in the production of turbulence kinetic energy and the eventual laminarization [6, 7]. This same decrease in turbulence kinetic energy causes the decrease in Nusselt number even in case the flow remains turbulent, as shown in Fig. 1.

Comparison with laminarization by acceleration

The turbulent boundary layer undergoes a reversion towards laminar flow when its free stream is accelerated severely [18]. This is again caused by the rapid decrease in the shear stress with the distance from the wall [6, 19]. The criterion for the occurrence of laminarization in the accelerated boundary layer is given by [18, 19]

$$K \equiv \frac{\nu}{U_m^2} \frac{dU_m}{dx} > 3 \times 10^{-6}. \quad (10)$$

Since the acceleration of the free stream is expressed as $a = U_m(dU_m/dx)$, the acceleration parameter can be rewritten as $K = a\nu/U_m^3$. On the other hand, in the case of combined forced and natural convection, the acceleration exerted on the fluid near the wall by the buoyancy force is $a' = g\beta(T_f - T_m)$, so the Grashof number is written as $Gr = a'D^3/\nu^2$. With regard to the balance of forces acting on the fluid very near the wall, the foregoing two accelerations are considered to be effectively the same. Thus, the acceleration parameter K is rewritten in terms of the Grashof number as $K = Gr/Re^3$. As a result, the condition (10) for the occurrence of laminarization in the accelerated boundary layer can be translated to its equivalence in the combined-convection framework as

$$Gr/Re^3 > 3 \times 10^{-6}. \quad (11)$$

The border of the above inequality is plotted by the two-dot-chain line in Fig. 3 and it turns out to be located between the discrimination equations (8) and (9). Furthermore, the calculated points of minimum heat transfer lie close to this borderline.

In the case of an accelerated turbulent boundary layer, though the shear stress decreases rapidly near the wall, it does not change sign but tends to zero with the distance from the wall. Thus, the turbulence kinetic energy is effectively being produced within a limited region near the wall. Then, if this energy production is suppressed under the fulfillment of the condition (10), the complete laminarization will possibly occur even at a relatively large Reynolds number. On the other hand, in the case of turbulent mixed convection, the shear stress changes sign, and will become a large negative value away from the wall when the Reynolds number is large. The turbulence energy production in this far-wall region would be large enough to sustain the flow as turbulent. Thus, the laminar regime does not make inroads into the turbulent mixed-convection region without limit, but the inroad is confined to a certain extent as shown in Fig. 3.

EXPERIMENTAL APPARATUS AND PROCEDURE

A schematic diagram of the experimental apparatus is shown in Fig. 4. It formed a closed loop that endured to pressures up to 5 MPa, with a circulation

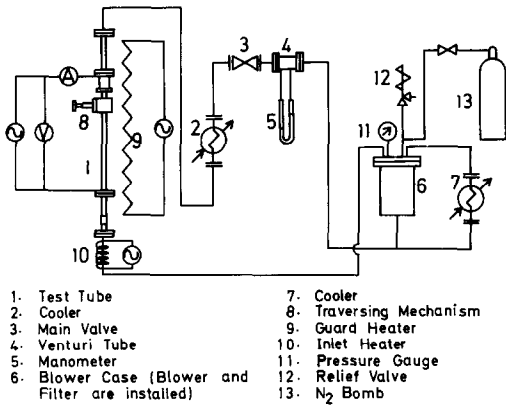


FIG. 4. Schematic diagram of experimental apparatus.

blower together with a motor installed in a pressure vessel. The nitrogen gas was circulated from the blower via the test-section, the cooler, the main valve, the venturi tube and then back to the blower. Figure 5 shows the details of the test-section. The test tube was made of a stainless-steel pipe of 23 mm I.D. and 27.2 mm O.D. The gas flow was provided with a definite inlet condition by an orifice with a diameter ratio $d/D = 10/23$. The heated length l of the test tube was $110D$. At a sufficiently downstream position from the start of heating ($x/D = 98$), the test tube was equipped with the hot-wire traversing mechanism which permitted a hot-wire sensor made of $5 \mu\text{m}$ tungsten wire to traverse the cross-section in the radial direction. A constant temperature anemometer together with a linearizer was employed to obtain

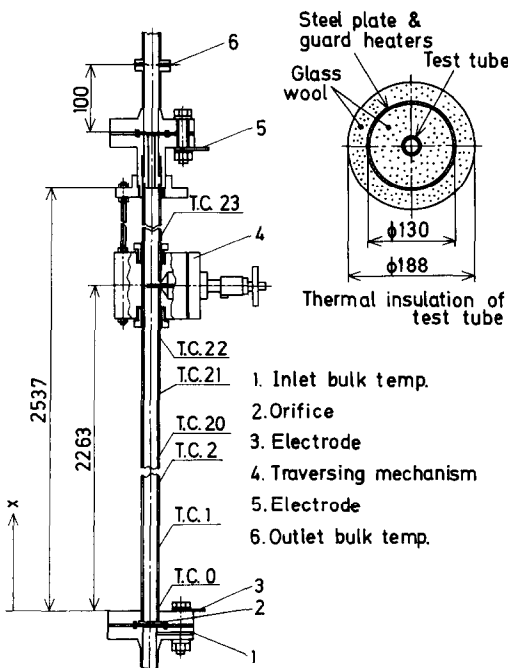


FIG. 5. Details of test-section.

signals related to streamwise velocity fluctuations. The inlet bulk temperature was measured by a chromel–alumel thermocouple just upstream of the inlet orifice. The outlet bulk temperature was measured after mixing the flow through a contraction–expansion section with a diameter ratio of $10/23$. For measuring wall temperature distributions, the test tube was fitted with 25 chromel–alumel thermocouples on the outer surface. The test-tube was heated by means of alternating current directly through it. The outside of the test-section was thermally insulated, covered first with thick glass-wool, then with an outer steel tube which was equipped with a guard heater system consisting of six individually-controllable ribbon heaters.

EXPERIMENTAL RESULTS AND COMPARISON WITH NUMERICAL PREDICTIONS

Heat transfer

Heat transfer measurements were performed with varying Grashof number under constant Reynolds numbers of 3000 and 5000 (see Table 1). In Fig. 6 wall temperature distributions along the test tube measured at three Grashof numbers at $Re = 3000$ are shown. The length of the entrance region changed considerably according to the experimental conditions, as is understood from Fig. 6. But, at a sufficiently downstream section, the flow and heat transfer were assumed to be fully developed, with the wall temperature varying almost parallel with the bulk temperature (the wall temperature distribution in the region of $x/D \geq 90$ was sometimes disturbed by maladjustment of the guard heater due to the existence of the large heat capacity of the hot-wire traversing mechanism). The mean wall-to-bulk temperature difference at the fully developed part was used to calculate the Nusselt and the Grashof numbers. Figure 7 shows the measured variations of the Nusselt number with the Grashof number, along with the numerical predictions of Kawamura’s model. The

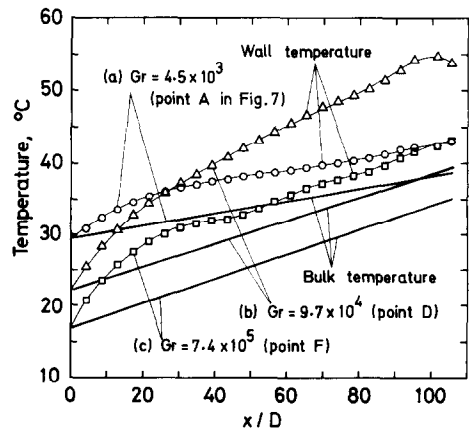


FIG. 6. Measured wall temperature distributions at three Grashof numbers under a constant Reynolds number of 3000.

Table 1. Experimental parameters (in the fully developed region)

No.	Point in Fig. 7	Re	Gr	Nu	U_m (m s ⁻¹)	q_w (W m ⁻²)	$T_w - T_m$ (K)	p (MPa)
301	A	3000	4.5×10^3	11.4	1.78	57	4.3	0.123
302	—	3000	8.7×10^3	11.7	1.27	56	4.1	0.169
303	—	3000	1.22×10^4	11.1	1.09	56	4.4	0.193
304	B	3000	2.7×10^4	7.7	0.97	71	7.9	0.22
305	C	2900	4.7×10^4	6.4	0.89	88	11.9	0.24
306	—	3000	7.9×10^4	6.3	0.67	77	10.5	0.33
307	D	2900	9.7×10^4	6.1	0.68	102	14.2	0.32
308	E	3000	2.6×10^5	6.5	0.38	80	10.6	0.58
309	F	3100	7.4×10^5	11.8	0.196	111	8.1	1.12
501	—	5000	2.2×10^4	15.1	1.41	78	4.5	0.25
502	—	5000	9.1×10^4	13.8	0.70	77	4.9	0.51
503	—	5000	2.2×10^5	11.7	0.54	94	6.9	0.65
504	—	5000	3.6×10^5	10.1	0.56	142	12.0	0.67
505	G	5000	6.3×10^5	8.4	0.26	45	4.7	1.29
506	—	5100	1.01×10^6	8.6	0.29	88	8.8	1.23
507	—	4800	1.65×10^6	10.0	0.25	147	12.3	1.43
508	H	5200	3.5×10^6	14.9	0.113	77	4.4	3.1
509	—	4800	9.4×10^6	17.3	0.076	134	6.3	4.6

data points with the lowest Grashof numbers fell well within the forced-convection regime, giving the Nusselt number close to Nu_0 . The corresponding wall temperature distribution [see curve (a) in Fig. 6] demonstrates that the heat transfer was fully developed within the range of approximately $x/D = 25$. With increase in the Grashof number, the Nusselt number decreased from Nu_0 , as predicted, and it exhibited a minimum value in the range from data point C to E for $Re = 3000$, this minimum occurred at point G in the case of $Re = 5000$. Keeping pace with this decrease in the Nusselt number, the entrance region for heat transfer got longer, as is clearly demonstrated by curve (b) in Fig. 6. As the Grashof number increased further, the Nusselt number increased and recovered to Nu_0 at point F in the case of $Re = 3000$, and at point H for $Re = 5000$. At this stage, a wavy pattern appeared in the wall temperature distribution [see curve (c) in Fig. 6], though it was not so pronounced as was reported for the case of supercritical fluids [3, 5].

Hot-wire measurements

Hot-wire anemometer measurements were made simultaneously with the heat transfer measurements

for the Reynolds number of 3000. Though the hot-wire traverse of the cross-section was made, the output signals obtained at a fixed sensor position of $y = 1.65$ mm from the pipe wall (corresponding to $y^+ = u^*y/\nu = 16$ under the pure forced-convection state) were chosen as representatives, and are shown in Fig. 8. The ordinate of Fig. 8 is the fluctuation V' of the anemometer output, nondimensionalized by the mean output at the pipe center V_c , while the abscissa is time t , nondimensionalized by the time scale D/U_m . If the flow was in a turbulent state, the fluid crossing the hot-wire sensor would naturally accompany temperature fluctuations. Fluctuations in the anemometer output voltage were, therefore, caused by fluctuations in both the velocity and the temperature. Here, the hot-wire anemometer was run at an over-heat ratio of 1.5, where the temperature difference between the sensor and the ambient fluid amounted to about 125°C. Compared with this, the wall-to-bulk temperature differences were relatively small, being about 10°C or less. Further, the linearizer was set so that in the case of isothermal flow almost linear characteristics between the output voltage and the flow velocity could be obtained. As a result it seems that

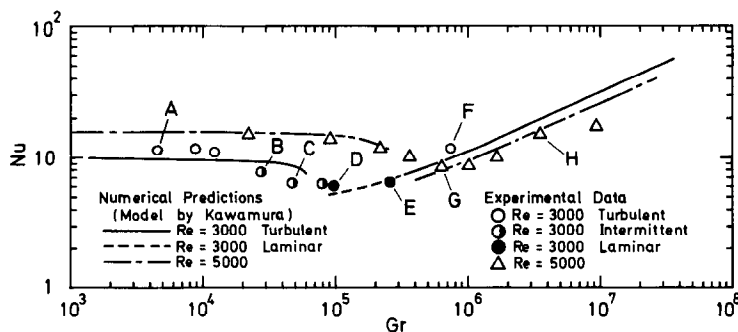


FIG. 7. Comparison between measured and predicted variations of Nusselt number with Grashof number.

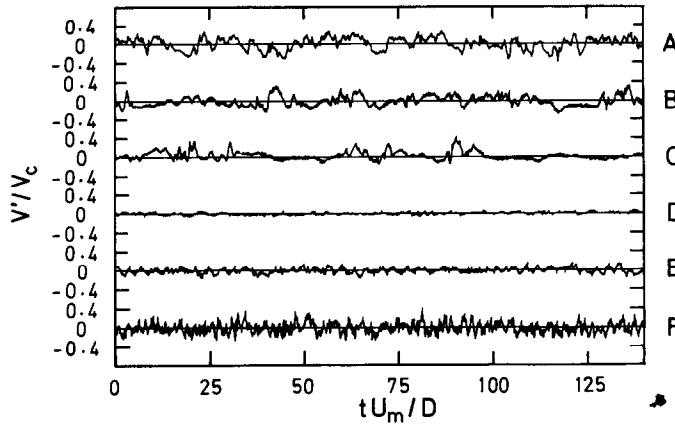


FIG. 8. Instantaneous signals of hot-wire placed at $y = 1.65$ mm, for various Grashof numbers under a constant Reynolds number of 3000: A, $Gr = 4.5 \times 10^3$; B, $Gr = 2.7 \times 10^4$; C, $Gr = 4.7 \times 10^4$; D, $Gr = 9.7 \times 10^4$; E, $Gr = 2.6 \times 10^5$; F, $Gr = 7.4 \times 10^5$.

the output signals in Fig. 8 reflected the velocity fluctuations acceptably well.

The uppermost signal A of Fig. 8, which corresponds to point A in Fig. 7, exhibits typical turbulent fluctuations. With increase in Grashof number, quiescent, supposedly laminar periods appeared intermittently in the signals (B–C in Fig. 8). At point D, where the minimum Nusselt number was brought about in Fig. 7, the flow became completely laminar, as can be seen from signal D in Fig. 8. With further increase in the Grashof number, turbulent fluctuations revived first at the region remote from the wall (E), and then active fluctuations spread to the near-wall region (F).

Regime map

The experimental results are summarized in the form of the regime map in Fig. 9. A symbol with a horizontal tick indicates the datum at the boundary between forced and mixed convection, while one with a vertical tick stands for the datum at the boundary between mixed and natural convection. The dis-

tinctions between the regimes were made by applying the same rule as was employed in the numerical predictions. The boundary points obtained in this way are in good agreement with the discrimination equations (8) and (9), hence, they also agree well with the boundaries predicted by the turbulence models. The laminar–turbulent distinction obtained by hot-wire measurements at $Re = 3000$ agrees very well with the prediction of Kawamura’s model. Thus, it has been experimentally demonstrated that the laminar regime makes inroads into the turbulent mixed-convection region.

CONCLUSIONS

Upward flow in a uniformly heated, vertical pipe (aiding flow) was studied, first by means of a numerical investigation utilizing the $k-\epsilon$ models of turbulence for low Reynolds number flows, and second by an experiment using nitrogen gas as a test fluid, whose pressure was changed in a range from atmospheric pressure to 5 MPa to cover four decades of the Gras-

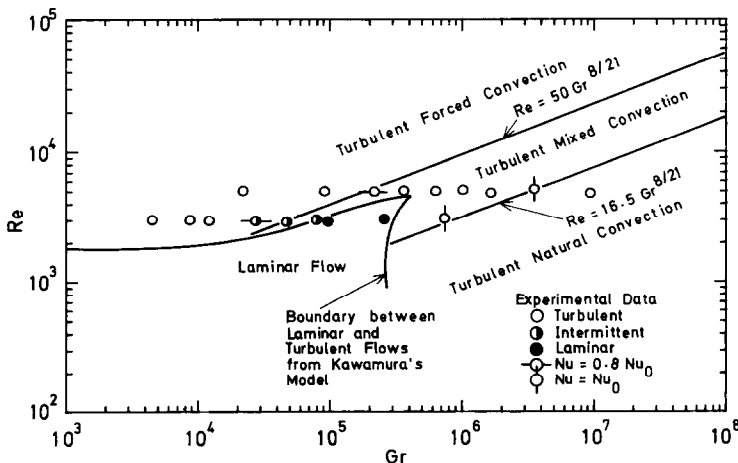


FIG. 9. Experimental data plotted on regime map for combined forced and natural convection.

hof number. Discriminations between forced, mixed and natural convections, as well as between laminar and turbulent flows were discussed in the Reynolds number against Grashof number plane. They are summarized in Figs. 3 and 9. The boundaries between forced, mixed and natural convections in the turbulent flow state, determined both by the numerical investigation and by the experiment, were in good agreement with the semi-theoretical equations (8) and (9) by Tanaka *et al.* [7, 8]. With regard to the boundary between laminar and turbulent flows, the numerical investigation predicted that the laminar regime made inroads into the turbulent mixed-convection region. This behavior was experimentally demonstrated. The reason for this behavior, being the same as the reason for heat transfer impairment in the mixed-convection regime, is attributed to the decrease in the production of turbulence kinetic energy which is caused by the rapid decrease in the shear stress with the distance from the wall.

Acknowledgement—The authors gratefully acknowledge the support for this work by the research grant (No. 60460108) of the Ministry of Education, Japan.

REFERENCES

1. B. Metais and E. R. G. Eckert, Forced, mixed, and free convection regimes, *J. Heat Transfer* **86**, 295–296 (1964).
2. E. R. G. Eckert and R. M. Drake, Jr., *Heat and Mass Transfer*, 2nd edn, pp. 331–332. McGraw-Hill, New York (1959).
3. M. E. Shitsman, Natural convection effect on heat transfer to a turbulent water flow in intensively heated tubes at supercritical pressures, *Proc. Inst. mech. Engrs* **182** (3D), 36–41 (1967–68).
4. M. J. Watts and C. T. Chou, Mixed convection heat transfer to supercritical pressure water, *Proc. 7th Int. Heat Transfer Conference*, Vol. 3, pp. 495–500, München (1982).
5. J. D. Jackson and W. B. Hall, Influences of buoyancy on heat transfer to fluids flowing in vertical tubes under turbulent conditions. In *Turbulent Forced Convection in Channels and Bundles* (Edited by S. Kakaç and D. B. Spalding), Vol. 2, pp. 613–640. Hemisphere, Washington, DC (1979).
6. W. B. Hall and J. D. Jackson, Laminarization of a turbulent pipe flow by buoyancy forces, ASME paper No. 69-HT-55 (1969).
7. H. Tanaka, A. Tsuge, M. Hirata and N. Nishiwaki, Effects of buoyancy and of acceleration owing to thermal expansion on forced turbulent convection in vertical circular tubes, *Int. J. Heat Mass Transfer* **16**, 1267–1288 (1973); *Trans. Japan Soc. mech. Engrs* **39**, 3394–3408 (1973), in Japanese.
8. H. Tanaka and T. Noto, Effect of natural convection on turbulent forced convection heat transfer in a vertical tube, *Proc. 10th National Heat Transfer Symposium*, pp. 225–228, Japan (1973), in Japanese.
9. J. D. Jackson and J. Fewster, Enhancement of turbulent heat transfer due to buoyancy for downward flow of water in vertical tubes. In *Heat Transfer and Turbulent Buoyant Convection* (Edited by D. B. Spalding and N. Afgan), Vol. 2, pp. 759–775. Hemisphere, Washington, DC (1977).
10. B. P. Axcell and W. B. Hall, Mixed convection to air in a vertical pipe, *Proc. 6th Int. Heat Transfer Conference*, Vol. 1, pp. 37–42, Toronto (1978).
11. A. M. Abdelmeguid and D. B. Spalding, Turbulent flow and heat transfer in pipes with buoyancy effects, *J. Fluid Mech.* **94**, 383–400 (1979).
12. H. O. Buhr, E. A. Horsten and A. D. Carr, The distortion of turbulent velocity and temperature profiles on heating, for mercury in a vertical pipe, *J. Heat Transfer* **96**, 152–158 (1974).
13. V. C. Patel, W. Rodi and G. Scheuerer, Turbulence models for near-wall and low Reynolds number flows: a review, *AIAA J.* **23**, 1308–1319 (1985).
14. W. P. Jones and B. E. Launder, The prediction of laminarization with a two-equation model of turbulence, *Int. J. Heat Mass Transfer* **15**, 301–314 (1972).
15. W. P. Jones and B. E. Launder, The calculation of low-Reynolds-number phenomena with a two-equation model of turbulence, *Int. J. Heat Mass Transfer* **16**, 1119–1130 (1973).
16. H. Kawamura, Analysis of transient turbulent flow using a phenomenological model of turbulence, *Proc. 21st National Heat Transfer Symposium*, pp. 40–42, Japan (1984), in Japanese.
17. S. V. Patankar, *Numerical Heat Transfer and Fluid Flow*. Hemisphere, Washington, DC (1980).
18. P. M. Moretti and W. M. Kays, Heat transfer to a turbulent boundary layer with varying free-stream velocity and varying surface temperature, *Int. J. Heat Mass Transfer* **8**, 1187–1202 (1965).
19. H. Tanaka, H. Kawamura, A. Tateno and S. Hatamiya, Effect of laminarization and retransition on heat transfer for low Reynolds number flow through a converging to constant area duct, *J. Heat Transfer* **104**, 363–371 (1982).

CONVECTION MIXTE DE CHALEUR POUR UN ECOULEMENT ASCENDANT DANS UN TUBE VERTICAL UNIFORMEMENT CHAUFFE

Résumé—On adopte le modèle $k-\epsilon$ pour prédire l'écoulement pleinement établi, ascendant dans un tube vertical chauffé uniformément, en tenant compte des forces d'Archimède. On détermine numériquement la cartographie des régimes pour les convections mixtes et naturelles, aussi bien que pour les écoulements laminaires et turbulents. En même temps, des expériences sont conduites à des nombres de Reynolds de 3000 et 5000, les nombres de Grashof variant largement, en utilisant de l'azote pressurisé comme fluide d'essai. En accord avec le calcul, le transfert de chaleur est mesuré dans le domaine de la convection mixte. De plus, à partir des mesures au fil chaud, on trouve une complète laminarisation dans la région de convection mixte à un nombre de Reynolds de 3000.

DER WÄRMEÜBERGANG BEI MISCHKONVEKTION FÜR AUFWÄRTSSTRÖMUNG IN EINEM GLEICHMÄSSIG BEHEIZTEN SENKRECHTEN ROHR

Zusammenfassung—Zur Berechnung der voll ausgebildeten Aufwärtsströmung in einem gleichmäßig beheizten senkrechten Rohr unter Berücksichtigung der Auftriebskraft wurde das k - ϵ -Turbulenzmodell für Strömungen bei kleinen Reynolds-Zahlen angewandt. Anhand der numerischen Berechnungen wurden sowohl für laminare als auch turbulente Strömungen Bereichskarten für erzwungene, gemischte und natürliche Konvektion erstellt. Zur gleichen Zeit wurden Versuche mit verdichtetem Stickstoff als Versuchsfluid bei Reynolds-Zahlen zwischen 3000 und 5000 in einem weiten Bereich von Grashof-Zahlen durchgeführt. In Übereinstimmung mit den Berechnungen wurde im Bereich der Mischkonvektion eine Beeinträchtigung des Wärmeübergangs durch die Auftriebsbewegung gemessen. Darüber hinaus wurde aufgrund von Hitzdrahtmessungen der vollständige Umschlag zur Laminarströmung im Bereich der Mischkonvektion bei einer Reynolds-Zahl von 3000 gezeigt.

ТЕПЛОПЕРЕНОС СОВМЕСТНОЙ ВЫНУЖДЕННОЙ И ЕСТЕСТВЕННОЙ КОНВЕКЦИЕЙ ПРИ ВОСХОДЯЩЕМ ТЕЧЕНИИ В РАВНОМЕРНО НАГРЕВАЕМОЙ ВЕРТИКАЛЬНОЙ ТРУБЕ

Аннотация—Для расчета полностью развитого восходящего потока в равномерно нагреваемой вертикальной трубе с учетом подъемных сил предложены k - ϵ модели турбулентности для течения с малым числом Рейнольдса. По данным численных расчетов построены графики течений для вынужденной, смешанной и естественной конвекций в ламинарном и турбулентном режимах. Одновременно при значениях числа Рейнольдса в диапазоне от 3000 до 5000 и при числе Грасгофа, изменяющемся в широком диапазоне, проводились опыты, в которых в качестве рабочей жидкости использовался азот. Измеренное ослабление теплообмена, вызванное подъемными силами в смешанном конвективном режиме, находится в соответствии с расчетами. Кроме того, термоанемометрическими измерениями показана полная ламинаризация в смешанной конвекции при числе Рейнольдса 3000.